Sādhanā Vol. 28, Parts 1 & 2, February/April 2003, pp. 187–208. © Printed in India

Cyclic deformation behaviour of austenitic steels at ambient and elevated temperatures

Th NEBEL and D EIFLER

Institute of Materials Science, University of Kaiserslautern, P.O. Box 3049, 67653 Kaiserslautern, Germany
e-mail: eifler@mv.uni-kl.de

Abstract. The aim of the present investigation is to characterise cyclic deformation behaviour and plasticity-induced martensite formation of metastable austenitic stainless steels at ambient and elevated temperatures, taking into account the influence of the alloying elements titanium and niobium. Titanium and niobium are ferrite-stabilising elements which influence the ferrite crystallisation. Furthermore, They form carbides and/or carbonitrides and thus limit the austenite-stabilising effect of carbon and nitrogen. Several specimen batches of titanium and niobium alloyed austenite and of a pure Cr-Ni-steel for comparison were tested under stress and total strain control at a frequency of 5 Hz and triangular load-time waveforms. Stress–strain-hysteresis and temperature measurements were used at ambient temperature to characterise cyclic deformation behaviour. Plasticity-induced martensite content was detected with non-destructive magnetic measuring techniques. The experiments yield characteristic cyclic deformation curves and corresponding magnetic signals according to the actual fatigue state and the amount of martensite. Fatigue behaviour of X6CrNiTi1810 (AISI 321), X10CrNiCb189 (AISI 348) and X5CrNi1810 (AISI 304) is characterised by cyclic hardening and softening effects which are strongly influenced by specific loading conditions. Martensite formation varies with the composition, loading conditions, temperature and number of cycles.

Keywords. Fatigue; cyclic deformation behaviour; metastable austenitic steel; plasticity-induced martensite.

1. Introduction

Owing to their excellent mechanical and technological properties, i.e. high toughness as well as their corrosion resistance, the investigated steels X6CrNiTi1810 (1·4541), X10CrNiCb189 (1·4546) and X5CrNi1810 (1·4301) are widely used, e.g. in power stations and in chemical plant constructions. In these applications, structural materials are usually subjected to variable temperature fields and corresponding high stress fields, which lead to fatigue. The term fatigue includes all microstructural changes in metallic materials occuring under cyclic loading. Most of the fatigue failures observed are a result of alternating cyclic loads or of cyclic loads superimposed by static mechanical loads under atmospheric conditions or combined

with thermal and/or corrosive environmental effects. Independent of the special loading conditions, which can be stress-or strain-controlled the fatigue process in all cases is connected with cyclic plastic deformations, crack initiation and crack propagation. The cyclic deformations cause microstructural changes in the materials connected with softening and/or hardening phenomena, characteristic dislocation structures, surface topographies, micro-cracks and finally macro-cracks. These fatigue stages are also present at higher temperatures. Nevertheless, thermally activated as well as time-dependent processes become more important with increasing temperatures (Eifler 2000).

In metastable austenitic steels due to plastic deformation local phase transformations of paramagnetic austenite in ferromagnetic martensite occur. The phase transformation of *fcc* γ-austenite to tetragonal distorted or *bcc* α'-martensite is characterised by unambiguous distinguishing marks. It is a transformation without diffusion of separate atoms. Dependent on the alloy composition, the austenite is converted directly or indirectly over the hexagonal ε-martensite into the α'-martensite. In case of a γ- to ε-transformation a volume reduction and with a γ- to α'-transformation a volume expansion occurs (Bayerlein *et al* 1989).

The effect of plasticity-induced martensite formation can be used for non-destructive testing methods. The transformation can be detected with high sensitive magnetic field sensors and be assigned to the plastic deformation and thus in good approximation to the actual state of fatigue damage. In order to be able to evaluate the results from non-destructive measurements correctly, it is necessary to describe the dependencies of the cyclic deformation behaviour and the microstructural changes in the bulk material in detail.

2. Materials

The steels were obtained as round bars with a diameter of 20 mm. Table 1 shows the chemical composition of the steels. The chemical analysis indicates that the investigated batch of the steel 1·4546 shows a higher carbon and a slightly decreased nickel content and corresponds therefore to the composition X6CrNiNb1810 (1·4550).

A large number of technically relevant chromium-nickel stainless steels after quenching from the solution annealing temperature exhibit austenite in metastable state. Their microstructural states can be represented either in a ternary temperature–concentration diagram or in the Schaeffler diagram (figure 1). Chrome and nickel equivalents consider the ferrite-or austenite-stabilising effect of the other alloying elements. Many highly alloyed austenitic steels are not in the three-phase regime of austenite, δ-ferrite and martensite in the Schaeffler diagram but occupy a position in the ternary temperature–concentration diagram in an area in which martensite is present as a stable phase. But due to their vicinity to the three phase regime, plastic deformation can lead to the formation of martensite (Eckstein 1990).

Table 1. Chemical compositon [weight-%].

Material	C	Si	Mn	Cr	Mo	Ni	V	W	Co	Cu	Nb	Ti	Al	N
1·4541	0·03	0·45	1·74	17·34	0·28	9·90	0·10	0·03	0·07	0·03	0·03	0·12	0·009	0·016
1·4546	0·04	0·41	1·54	17·41	0·26	9·29	0·12	0·03	0·08	0·03	0·37	0·02	0·015	0·022
1·4301	40·03	0·58	1·75	18·42	0·37	9·05	0·09	0·05	0·06	0·03	0·03	0·02	0·007	0·050

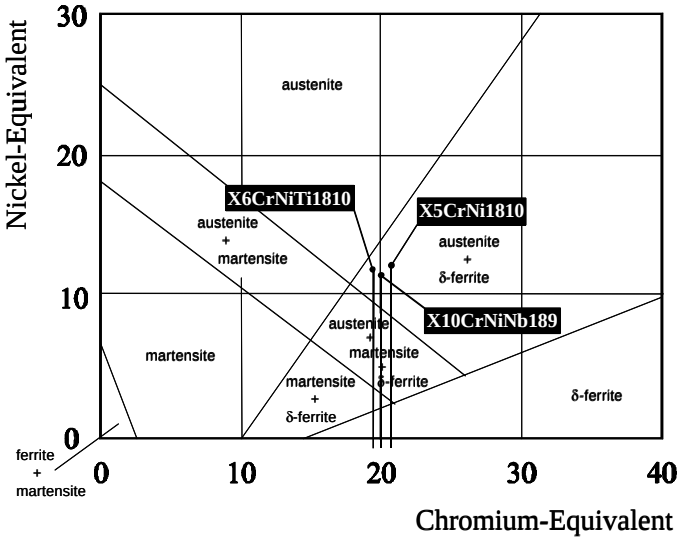

Figure 1. Schaeffler-diagram.

The chromium and nickel equivalents of various steels indicated in figure 1 are:

$$\text{Chromium-equivalent: } 1\text{Cr} + 2\text{Si} + 1{\cdot}5\text{Mo} + 5\text{V} + 5{\cdot}5\text{Al} + 1{\cdot}75\text{Nb} + 1{\cdot}5\text{Ti} + 0{\cdot}75\text{W}. \quad (1)$$

$$\text{Nickel-equivalent: } 1\text{Ni} + 1\text{Co} + 0{\cdot}5\text{Mn} + 30\text{C} + 0{\cdot}3\text{Cu} + 25\text{N}. \quad (2)$$

$$\Rightarrow \text{X6CrNiTi1810}: \text{ Cr-equivalent} = 19{\cdot}46, \text{ Ni-equivalent} = 12{\cdot}15,$$

$$\Rightarrow \text{X10CrNiNb189}: \text{ Cr-equivalent} = 20{\cdot}00, \text{ Ni-equivalent} = 11{\cdot}90,$$

$$\Rightarrow \text{X5CrNi1810}: \text{ Cr-equivalent} = 20{\cdot}74, \text{ Ni-equivalent} = 13{\cdot}38.$$

Figure 2 gives a thermodynamic interpretation of phase stability as a function of free enthalpy and temperature. To induce phase transformation a certain undercooling of ΔT below T_o is necessary. The martensite start temperature 'M_S' for most of the austenitic steels is well below room temperature, however, it can be shifted to substantially higher temperatures by plastic deformation (Bassler *et al* 1997). The deformation-induced martensite formation is promoted after attaining a critical plastic-strain at the temperature M_d. The determination of this temperature is difficult. In view of this the so-called M_{d30}-temperature is usually determined. This temperature corresponds to 50% martensite formation due to 30% deformation (Eckstein 1990).

$$\text{M}_\text{S}[^\circ C] = 1350 - 1665(\text{C} + \text{N}) - 28\text{Si} - 33\text{Mn} - 42\text{Cr} - 61\text{Ni}, \quad (3)$$

$$\text{M}_{\text{d30}}[^\circ C] = 497 - 462(\text{C} + \text{N}) - 9{\cdot}2\text{Si} - 8{\cdot}1\text{Mn} - 13{\cdot}7\text{Cr} - 20\text{Ni} - 18{\cdot}5\text{Mo}. \quad (4)$$

After austenitizing and quenching in water steels with less than 16% of nickel exhibit metastable state between ambient temperature and the temperature of liquid helium, i.e. phase transformations with or without diffusion can occur (Olsen & Cohen 1975). The austenite stability can be estimated with different empirical relations. The required nickel content can be calculated with the following equations.

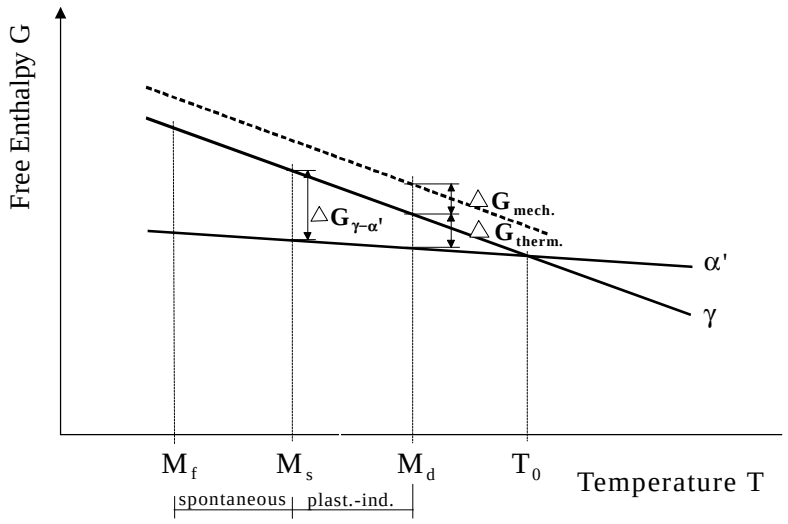

Figure 2. Free-enthalpy–temperature diagram.

$$Ni_{th}[\%] = [(Cr + 1{\cdot}5Mo - 20)/12] - (Mn/2) - 35C - 27N - Cu + 15, \quad (5)$$

$$\Delta Ni = N_{anal.} - Ni_{theor.} \quad (6)$$

The difference between the analytically determined nickel content and theoretical content is used as a characteristic value for austenite stability (Eckstein 1990). An alloy with negative difference becomes more metastable with an increasing amount of the difference, ΔNi (table 2).

The quasi-static characteristic values indicated in table 2 refer to the solution-annealed material (1050°C for 35 min and quenched in water).

Prior to fabrication of specimens, a well-defined thermal treatment is necessary to eliminate the effects of earlier processing routes. The semi-finished bars of 1·4541 and 1·4301 were cold-rolled contrary to the hot-rolled 1·4546. The tensile strength and the yield strength with 1 percent plastic deformation are in the lower range of the required values.

3. Experimental procedure

The experiments were performed on a 100 kN servohydraulic testing machine under stress and total strain control with a frequency of 5 Hz and triangular load-time functions. The tests were stopped after failure or after reaching 2 million cycles whichever was earlier.

Table 2. Characteristic data of the difference in nickel content of investigated steels.

Material*	ΔNi	M_s[°C]	M_{d30}[°C]	R_m[MPa]	$R_{p1,0}$[MPa]	A_s[%]
1·4541	−2·53	−129	17	588	243	36·9
1·4546	−2·73	−113	23	655	300	33·5
1·4301	−2·56	−183	0·3	617	287	39·2

*solution: 1050°C/35 min/H_2O

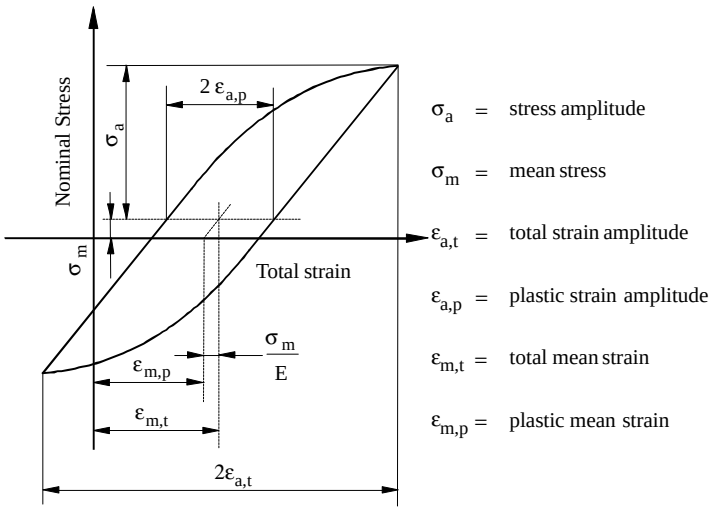

Figure 3. Characteristic values of a hysteresis loop.

3.1 *Stress–strain-hysteresis measurement*

The characterization of the cyclic deformation behaviour is carried out by recording stress–strain hysteresis loops. Figure 3 shows the characteristic values of a hysteresis loop for elastic-plastic deformation with $\sigma_m > 0$ MPa. Under cyclic loading, and at amplitudes above the fatigue limit, microstructural processes change the stress-strain-relationship in a characteristic manner and cause crack initiation after a certain number of cycles. It is a common practice to use cyclic deformation curves where the plastic-strain amplitude is plotted as a function of the number of cycles to describe the cyclic deformation behaviour of metallic materials.

Figure 4 shows a sequence of the basic diagrams which can be used to assess the fatigue behaviour of metallic materials. The macro-crack-free regime normally is characterised by cyclic deformation curves (see figure 4a) and if cyclic saturation occurs, then the relation between loading stresses (strains) and the resulting strains (stresses) remains approximately constant and cyclic stress-strain curves (see figure 4b) can be derived. After micro-crack initiation, the further fatigue process can be quantitatively described by crack growth curves (see figure 4c), and finally the relation between loading amplitudes and the number of cycles to macro-crack initiation or failure is given by stress or total-strain Wöhler-curves (see figure 4d) (Eifler 1997).

3.2 *Temperature measurement*

With different methods for the measurement of specimen temperature during cyclic loading cyclic-stress–temperature-curves can be determined similarly to the common cyclic-stress–strain-curves. With this method in the range of macroscopically quasi-elastic deformation additional information about microstructural processes can be detected (Harig & Dengel 1980). To realize an accurate temperature measurement, three thermocouples were used (see figure 5). The specimens were clamped in thermostatically-controlled wedge grips. This is necessary to avoid temperature gradients in the specimens caused by the servohydraulic test system. The cross sections with the thermocouples T_2 and T_3 are bigger in diameter in

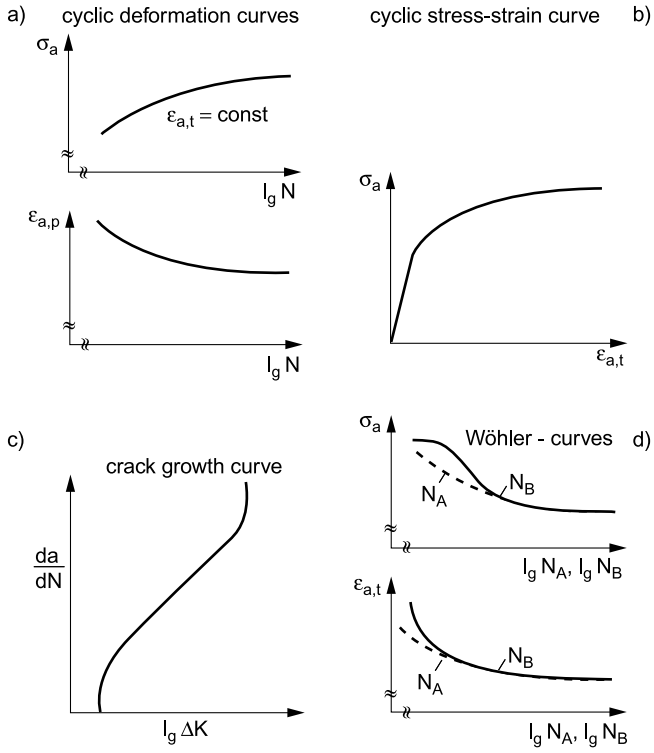

Figure 4. Basic diagrams.

comparison with the one in the gauge length (T_1). So it is safe to assume that temperature changes are only caused by plastic deformations in the gauge length itself. ΔT as T_1 minus the mean value of T_2 and T_3 is independent of any temperature changes that concern the whole specimen e.g. like changes in ambient temperature (see figure 6).

3.3 *Magnetic measurement*

3.3a *FerriteScope:* Plasticity-induced martensite formation at ambient temperature was detected *in situ* with a commercially available FerriteScope, which is calibrated to measure the ferrite content of weldments. Therefore the magnetic fraction is indicated in %-ferrite.

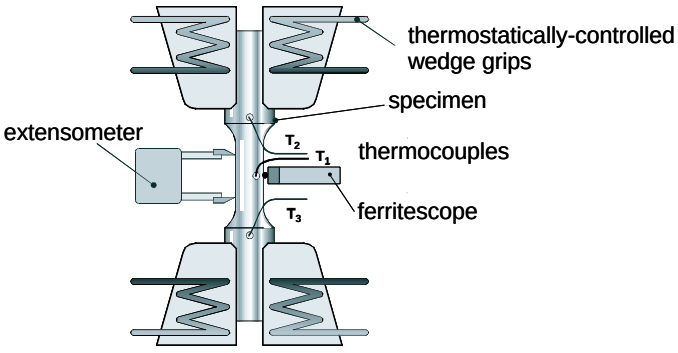

Figure 5. Position of sensors.

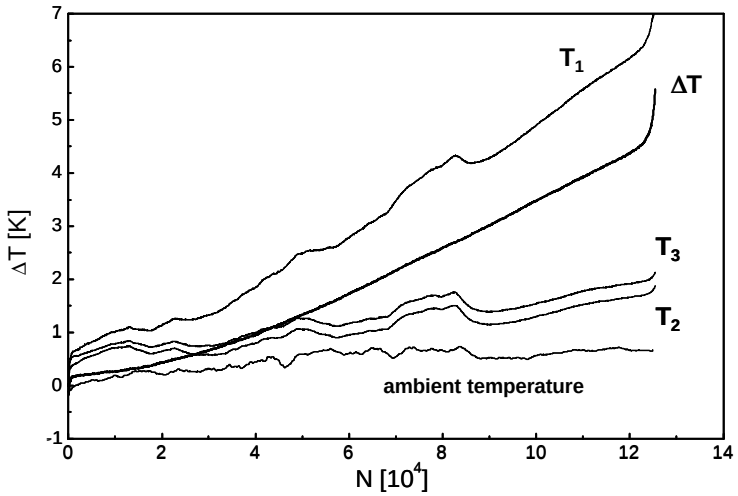

Figure 6. Thermocouple signals. Change of temperature: $\Delta T = T_1 - 0{\cdot}5(T_2 + T_3)$ [K].

Due to the measurement principle the detection depth of the assigned single-pole measuring probe depends on the magnetic phase. The probe forms a magnetic circuit when it is placed on the specimen and excited by a low-frequency magnetic field. The voltage induced in the probe coil by this field is a direct measure of permeability. The device allows the determination of ferrite content upto approximately 7% to a depth of 3 to 3·5 mm. The output signal of the FerriteScope (approx. 4 values/s) is recorded together with the values of the temperature measurement (Nebel *et al* 2001).

3.3b *SQUID measurement:* As the martensite fraction is extremely low for in-service temperatures of about 300°C highly sensitive measuring systems are necessary. In order to have a chance to measure very small amounts of martensite a SQUID-magnetometer developed from ISI, Forschungszentrum Jülich, Germany was used (figure 7).

Systems on the basis of HTC-SQUIDs (high temperature superconducting quantum interference devices) combine a higher sensitivity than fluxgate-sensors with a higher practicability than low-temperature SQUIDs cooled with liquid nitrogen. The aim was to measure the remanent magnetization of the specimens out of a definite distance from the SQUID and to obtain information about the amount of plasticity-induced martensite in the austenitic matrix (Lang *et al* 2000).

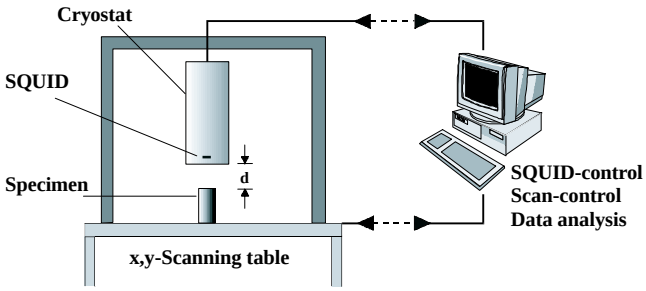

Figure 7. SQUID-magnetometer.

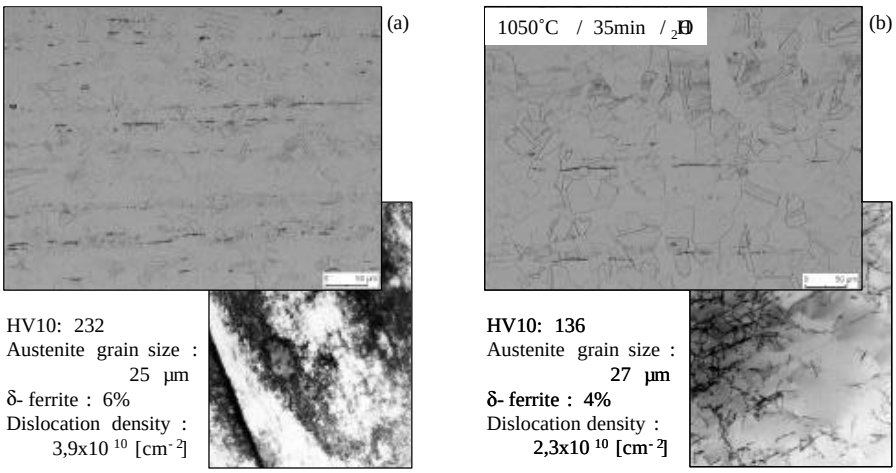

Figure 8. Micrographs. **(a)** Virgin state, **(b)** annealed solution.

3.3c *GMR-measurement:* Commercial GMR sensors have been used. The GMR effect, developed in 1988, is based on the magnetic field sensitivity of the electrical resistance of multi-layered magnetic and paramagnetic layers of only some nm thickness where spin-coupling (parallel/antiparallel) influences the scattering of the conduction electrons at the interfaces. For the applied GMR microchip four of these magnetoresistors are combined in a Wheatestonebridge. Using the GMR as a magnetor provides the same results as the SQUID. As it is not that sensitive, the distance to the specimen has to be smaller. A sensor-system was developed from Fraunhofer-Institut Zerstörungsfreie Prüfverfahren, Saarbrücken, Germany for on-line monitoring allowing simultaneous measurements of the static magnetic field as well as of the GMR-impedance (Dobmann *et al* 2001).

4. Results

4.1 *Microstructure*

Figure 8 shows light- and TEM-micrographs of X6CrNiTi1810 in as-delivered and solution annealed conditions. The Vickers hardness values, in the dislocation densities and the measured delta ferrite values deduced from the Schaeffler diagram are also indicated in figure 8.

A few aligned slag inclusions and δ-ferrite-lines were noticed in the rolling directions. Due to the solution annealing the hardness from the as delivered condition of 230 HV10 is reduced to 136 HV10 and the austenite grain size remained almost identical at a level of $\sim 25\mu$m.

4.2 *Multiple-step-tests at ambient temperature*

For a first orientation regarding the deformation behaviour stress controlled multiple step tests were performed (figure 9). The tests started at a quasi damage-free load level of 90 MPa (4 kN) and the value was increased stepwise by 0·5 kN every half an hour. The tests indicate that the deformation behaviour of the investigated steels is similar and is not influenced by

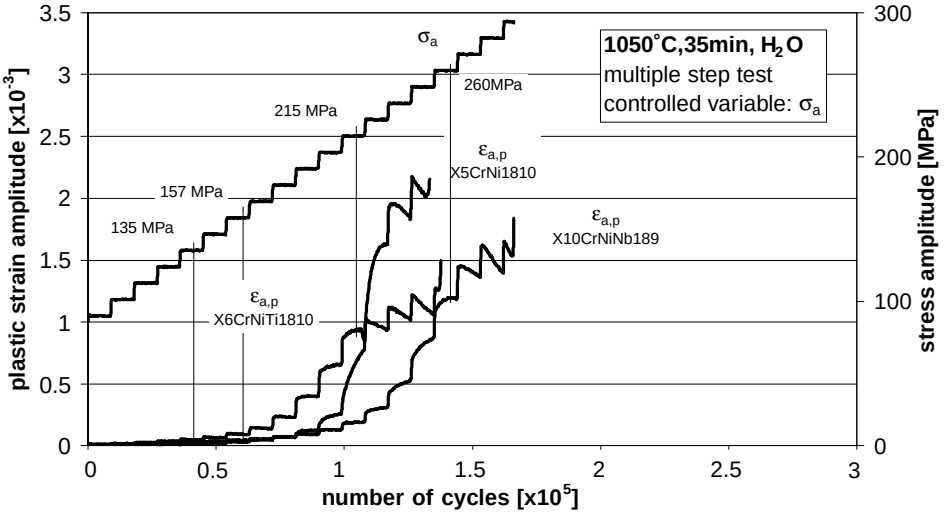

Figure 9. Results of the multiple step test.

the initial condition of the material. Furthermore it was possible to estimate the endurance limit with a sufficient accuracy to select suitable load amplitudes for the single-step-tests.

4.3 *Total-strain controlled single-step-tests at ambient temperature*

The steels were loaded with total-strain amplitudes from $2{\cdot}5 \times 10^{-3}$ to $3{\cdot}75 \times 10^{-3}$. The selected spectrum covers the area of fatigue strength and the endurance limit. In the following diagrams the cyclic deformation curves of the steel X10CrNiNb189 are represented, as well as the change of temperature and the development of the magnetic fraction versus the number of cycles. At the beginning of cyclic loading the three steels show a more or less pronounced hardening followed by a quasi-saturation or a very weak softening. With the amplitude of $2{\cdot}5 \times 10^{-3}$, all steels were cycled below their endurance limit. Particularly at low and middle total-strain amplitudes a secondary hardening occurs. A significant influence of the chemical composition in particular the ferrite-stabilizing alloying elements titanium and niobium on the cyclic deformation behaviour of the steels could not be determined under total-strain control. Figure 10b shows that the change of temperature curves cannot resolve the primary hardening. In contrast the cyclic softening which is only weakly visible in the cyclic deformation curves is clearly evident in the temperature measurement. A comparison of the cyclic deformation curves with the development of the magnetic fraction in figure 10c proves that the secondary hardening is attributed to the formation of α'-martensite. The martensite formation presupposes a certain amount of accumulated plastic-strain. This value is achieved after 10^3 cycles. Besides the absolute value of the plastic-strain amplitude, the accumulated plastic-strain, the number of cycles and the temperature are decisive. It must be differentiated between the change of specimen temperature due to the cyclic loading and the influence of the chosen test temperature. Higher test temperatures lead to lower martensite contents due to higher austenite stability. The comparison of figures 10b and 10c shows the influence of the specimen temperature induced by the plastic deformation. The small martensite contents with increasing total-strain amplitudes are associated with the higher specimen temperatures.

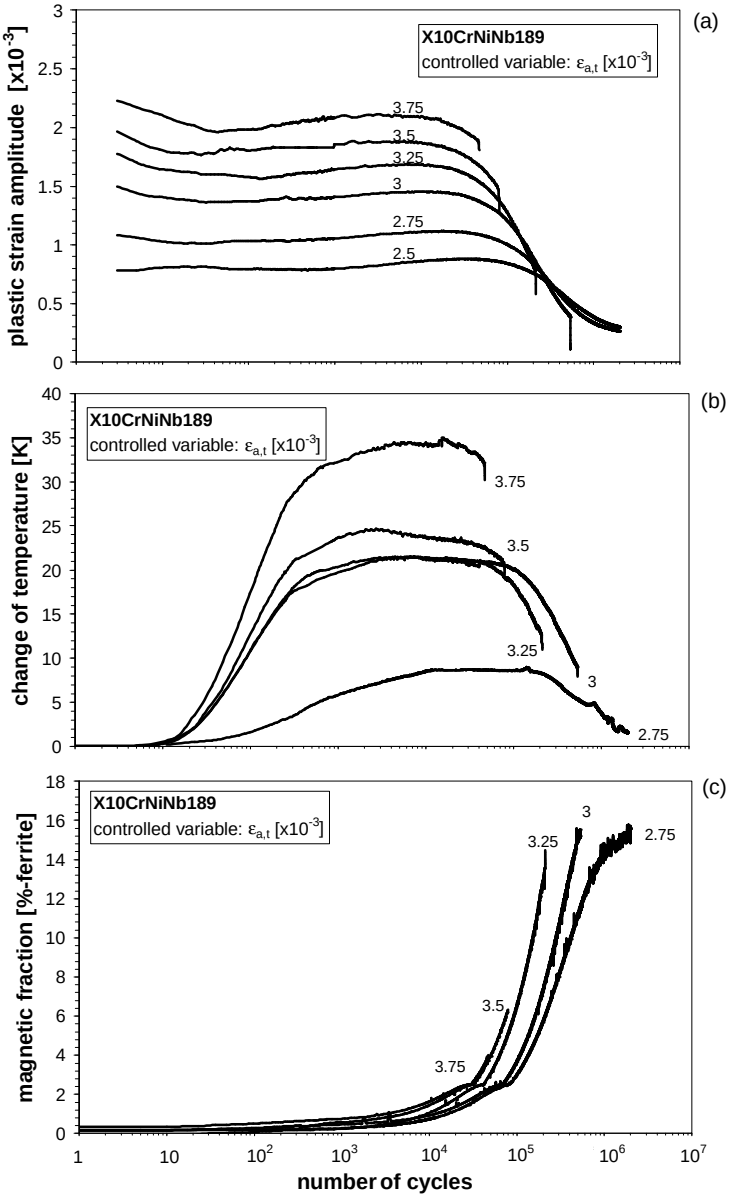

Figure 10. Results of total-strain controlled fatigue tests (X10CrNiNb189).

4.4 *Stress control*

4.4a *Stress-controlled single-step-tests at ambient temperature:* The stress controlled cyclic deformation curves compared with the total-strain controlled ones show clearly stronger marked hardening and softening effects.

Steel X6CrNiTi180 (see figure 11) indicates cyclic softening followed directly by cyclic hardening during the first 100 cycles; 2×10^6 cycles are achieved by steels X5CrNi1810 at

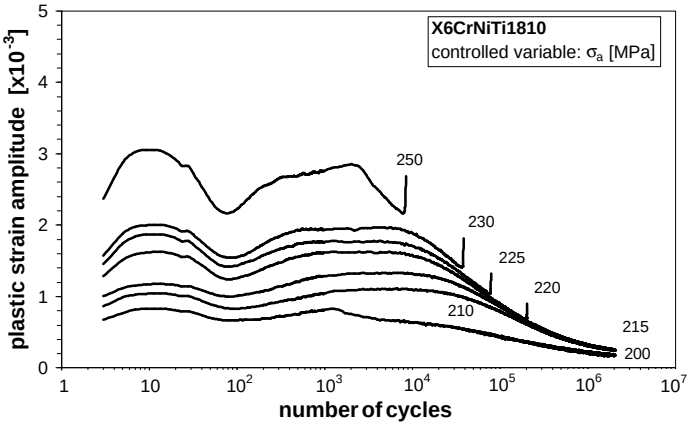

Figure 11. $\varepsilon_{a,p}$, N-curves of stress controlled fatigue tests (X6CrNiTi1810).

210 MPa and X6CrNiTi1810 at 215 MPa. Steel X10CrNiNb189 yields a higher endurance limit of about 260 MPa.

Evaluation of the fatigue strength has to take place dependent on the specific application. In case of a desired strength increase by the plasticity-induced martensite formation the niobium-alloyed metastable austenite should be used. If great variation of the magnetic properties of the material cannot be tolerated, titanium-alloyed steel with a smaller fatigue strength but a higher austenite stability should be preferred.

Figure 12 shows the change of temperature and the development of the magnetic fraction vs. the number of cycles for the steel X10CrNiNb189. The changes of temperature after an interval of 20 to 30 cycles and the plastic-strain amplitudes can be used in stress controlled tests as equivalent for the characterization of the cyclic deformation behaviour. The martensite formation already starts after 10^2 cycles but the absolute values are smaller about the factor 4 compared with total-strain control. Higher stress amplitudes generally lead to an earlier formation of martensite and higher martensite formation rates (see figure 12b).

4.4b *SQUID-measurements at ambient and elevated temperature:* In figure 13 characteristic results of the SQUID-measurements are plotted. Two batches of specimens of X6CrNiTi1810 (virgin state) at RT and $T = 300^\circ$C were investigated in defined states of magnetization. Cylindrical samples representing the actual fatigue state were taken from the gauge length of the specimens after different numbers of cycles. First experiments revealed that those specimens behave like magnetic dipoles. The remanent magnetization of these specimens is plotted together with the plastic-strain amplitude as a function of the life-time fraction (figure 14).

As expected the magnetic field values are much higher for the RT-samples than for those fatigued at $T = 300^\circ$C. This is caused by the much higher volume fraction of martensite at RT compared to $T = 300^\circ$C. The smaller amount of martensite is also the reason for the only slight changes of the plastic-strain amplitude at $T = 300^\circ$C.

4.4c *Results of GMR-measurements at ambient and elevated temperature:* The measurements show a clear correlation of the GMR-impedance with the plastic-strain amplitude under stress control. The GMR-impedance is influenced by the martensite content, the dislocation

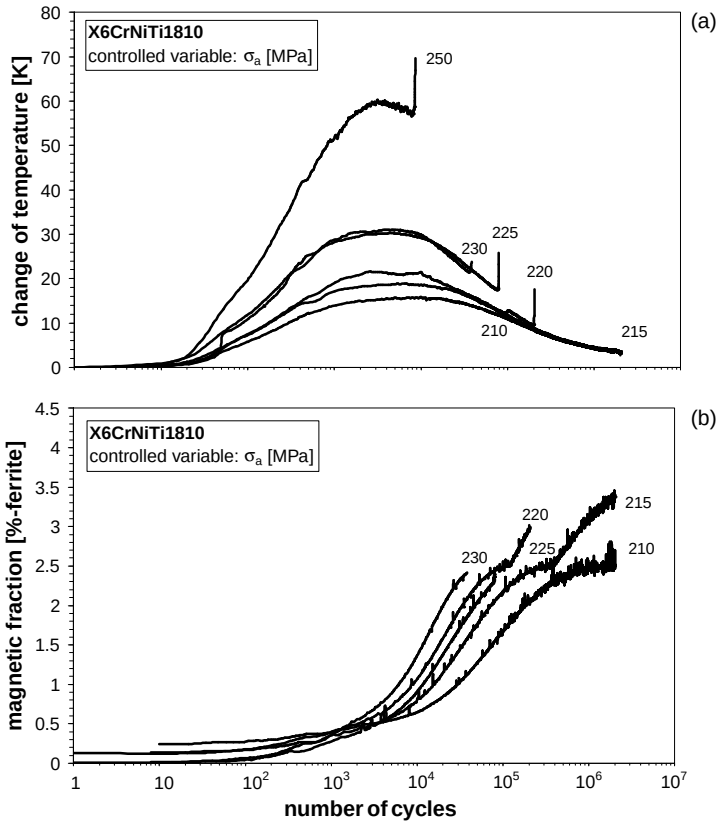

Figure 12. Change of temperature and development of the martensite quota (X6CrNiTi1810).

density and structure as well as the stress state. On-line monitoring of the fatigue tests were performed not only in single-step-tests at different stress amplitudes, but also in tests with a

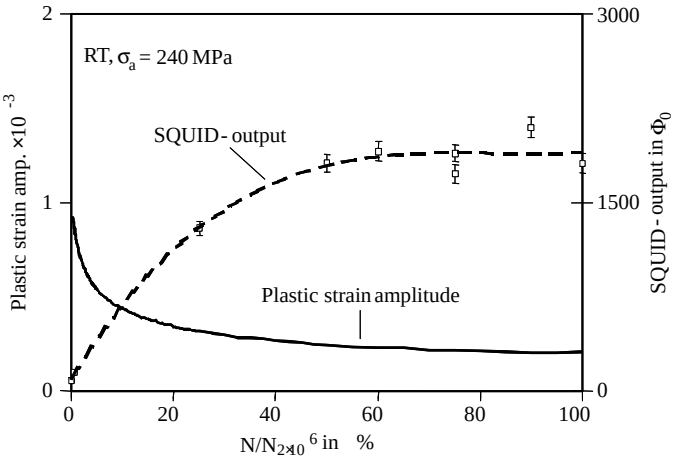

Figure 13. Remanent magnetization vs. cycles at ambient temperature (X6CrNiTi1810).

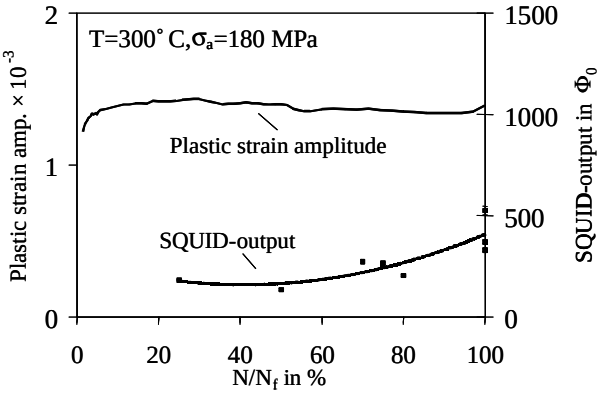

Figure 14. Remanent magnetization vs. cycles at elevated temperature (X6CrNiTi1810).

multiple-step loading mix of increasing and decreasing stress amplitudes. Figure 15 shows a characteristic result, for variable amplitude loading.

Impedance as a function of the cycles develops an increasing off-set which is an indication of the increasing martensite formation. Superimposed is an alternating signal following the plastic-strain amplitude due to the magneto-elastic effect.

4.5 *Mean load effects*

The influence of mean stresses on the cyclic deformation behaviour and the development of the magnetic fraction was evaluated with mean stresses of $\sigma_m = +45, +90$ and $+100$ MPa and -30 and -100 MPa. The plastic-strain amplitudes are arranged on characteristic levels in a relatively narrow band (see figure 16a). Positive mean stresses lead to higher plastic-strain amplitudes and decreasing number of cycles to failure, negative mean stresses lead to lower plastic-strain amplitudes and consequently increasing numbers of cycles to failure. The development of the martensite fraction ratio is comparable to tests without mean stresses. The transformation starts at about 200 cycles for positive mean stresses and this value increases up to 10^4 cycles for negative mean stresses proportional to the induced plastic-strain amplitudes (see figure 16b). For the investigated mean stresses cyclic creep behaviour was observed (see figure 16c). As expected, positive mean stresses lead to positive plastic mean

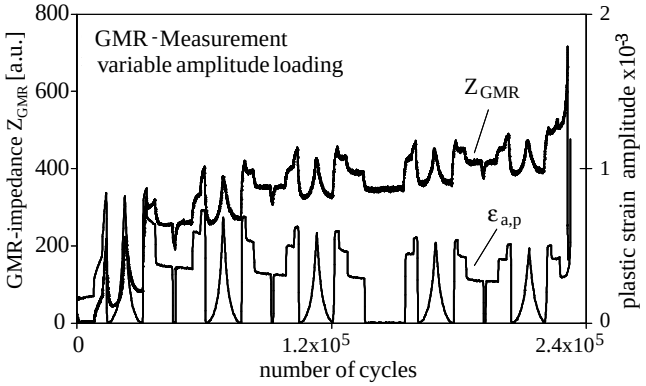

Figure 15. GMR-impedance vs. cycles (X6CrNiTi1810).

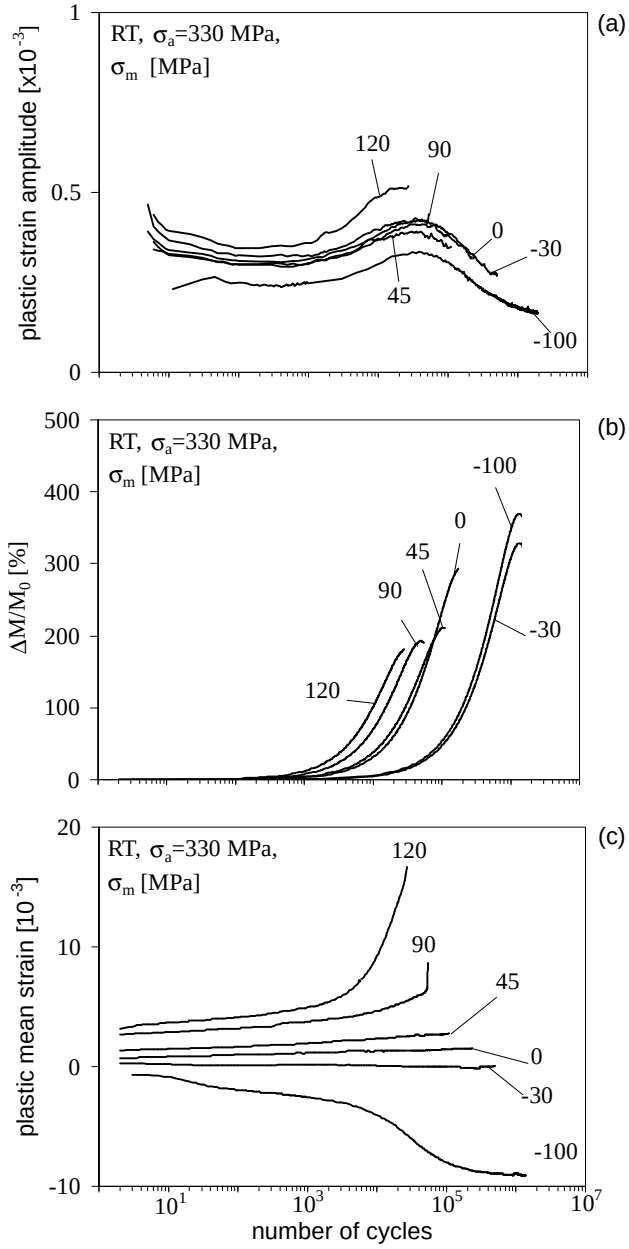

Figure 16. Results of fatigue tests with mean stress (X6CrNiTi1810).

strains and negative mean stresses to negative plastic mean strains and a shortening of the specimens.

For the investigated mean strains of $\varepsilon_{m,t} = +0{\cdot}5, +/-1{\cdot}5$ and $+/-2{\cdot}5 \times 10^{-3}$ the plastic-strain amplitudes are arranged in a narrow band and show independent of the mean strains nearly identical values. A significant influence of positive or negative mean strains on the martensite formation could not be determined, due to the fast and nearly complete relaxation of the mean stresses as shown in figure 17.

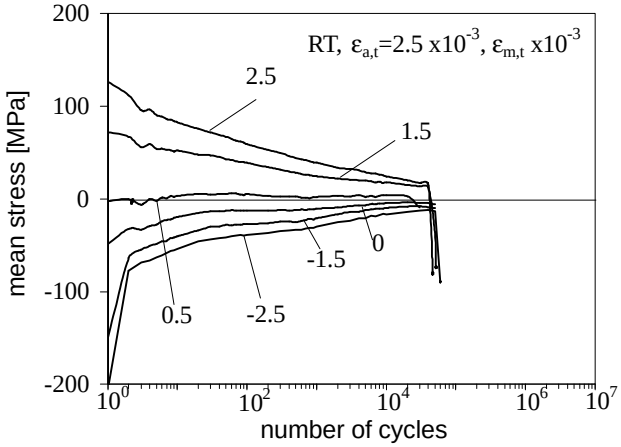

Figure 17. Results of fatigue tests with mean strains (X6CrNiTi1810).

4.6 *CSx-curves (stress control)*

The diagram in figure 18a contains the cyclic stress-strain (CSS) curves of the stress controlled single step tests of all three steels including the curve functions according to the power law of Morrow. The relevant values were taken at the half numbers of cycles to failure N_f. The cyclic strength coefficients correspond approximately to the determined endurance limits. The more pronounced martensite formation of the steel X10CrNiNb189 at higher stress amplitudes is reflected by a larger strength exponent. Furthermore presented CSS-curves underline the importance of the temperature measurement for the evaluation of the cyclic deformation behaviour (see figure 18b).

4.7 *CTSx-curves (total-strain control)*

An analysis of the total-strain controlled experiments presented in § 4·6 leads to decreasing CSS- and CST-Curves (see figure 19).

The reason for this behaviour is the strong secondary hardening already addressed due to pronounced martensite formation at low and middle total-strain amplitudes. Decreasing plastic-strain amplitudes cause under total-strain control an increase of the elastic strain and consequently the stress amplitude (see figure 20).

To value this kind of material behaviour the stress amplitude was replaced through the total-strain amplitude as the actual controlled variable. This method results in cyclic total stress-strain-curves with as expected higher plastic-strain amplitudes with increasing total-strain amplitudes and appropriate cyclic total strain-temperature-curves (see figure 21).

4.8 *Microstructure and surface features at ambient and elevated temperatures*

For the characterization of microstructural changes in the investigated steels, due to quasi-static and cyclic deformation, selected specimens were examined with light and electron microscopic and analytic procedures. Total-strain controlled tests were conducted at $\varepsilon_{a,t} = 3{\cdot}25 \times 10^{-3}$ and the samples were taken at 25, 50, 75 and 100% of the numbers of cycles to failure. Qualitative microscopic investigations were carried out as well as quantitative measurements of the formed martensite content and the dislocation density and structure were made. The development of the microstructural changes is comparable in the as delivered and

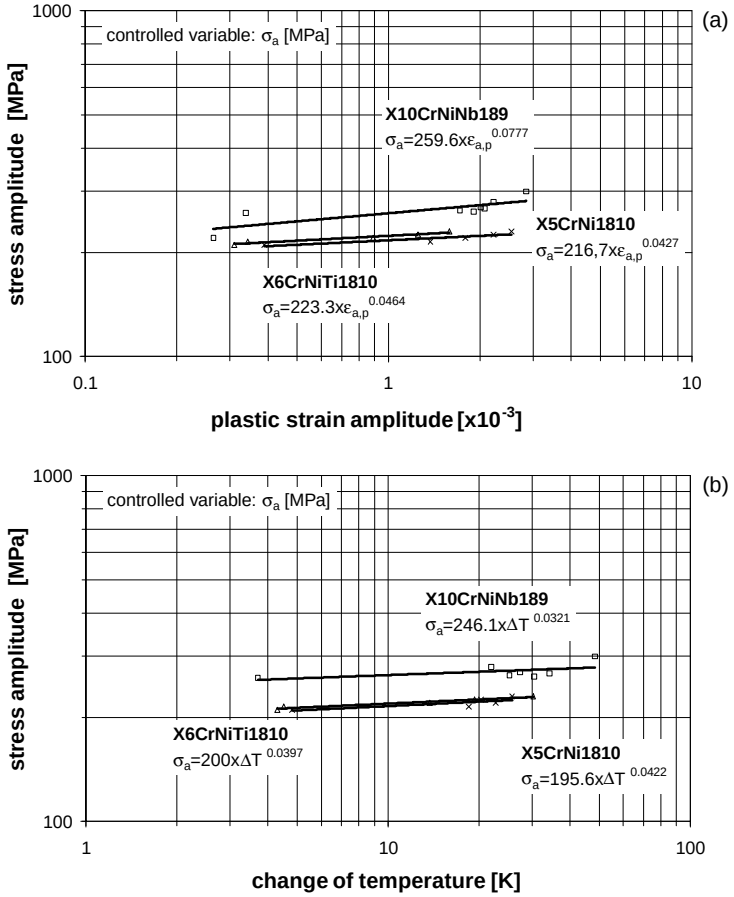

Figure 18. CSx-curves (stress control).

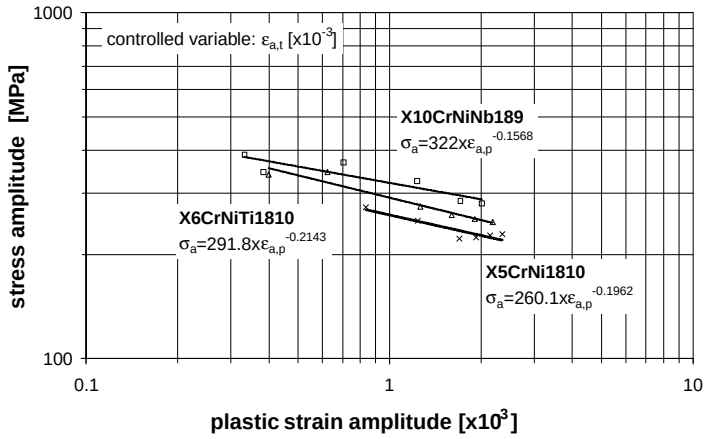

Figure 19. CSS-curves (total-strain control).

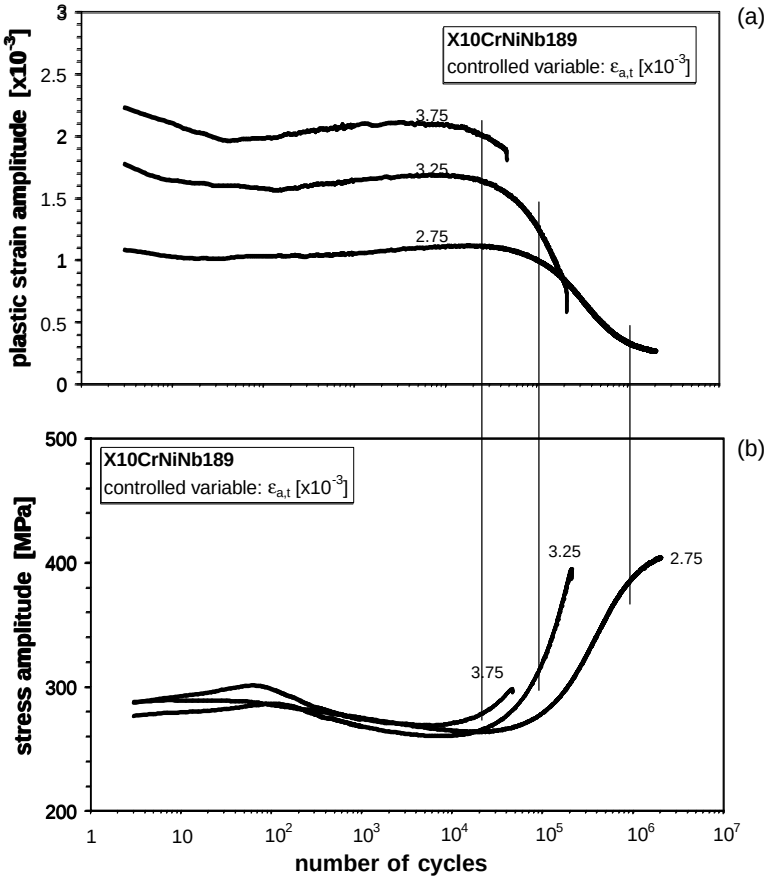

Figure 20. Determination of the values for the CSS-curve of X10CrNiNb189.

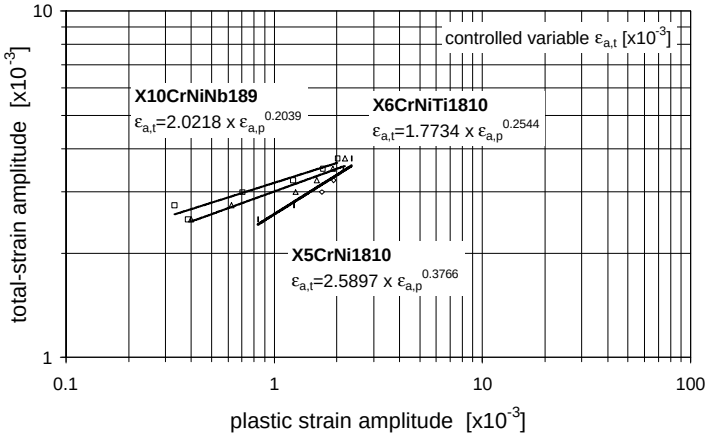

Figure 21. CTSS-curves (total-strain control).

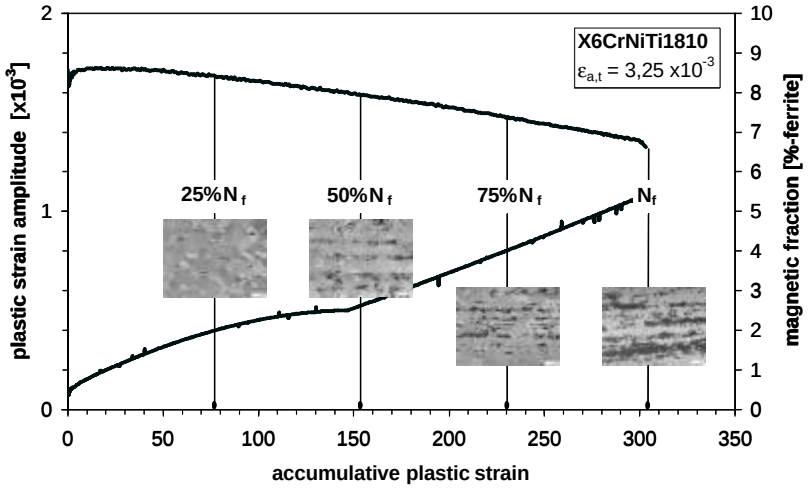

Figure 22. Microstructure of X6CrNiTi1810 at $3{\cdot}25 \times 10^{-3}$.

in the solution-annealed states. Figure 22 depicts the $\varepsilon_{a,p}$,-N-curve of X6CrNiTi1810, the change of the magnetic fraction vs. the accumulate plastic-strain and further the appropriate micrographs. With increasing number of cycles the analytically determined area fraction of the martensitic phase rises from 3 to 12, 13 and finally 34 area-%. The aligned slag inclusions in transformation direction cause local fluctuations in austenite stability and are suitable starting points for the martensite formation. All steels indicate an alignment of the martensite in rolling direction.

The microstructure reveals the influence of the alloying elements titanium and niobium on the martensite formation under total-strain control. In comparison with the steel X6CrNiTi1810 the X10CrNiNb189 forms clearly more martensite at the total-strain amplitude $3{\cdot}25 \times 10^{-3}$ in the first and last quarter of the life-time (see figure 23). The appropriate

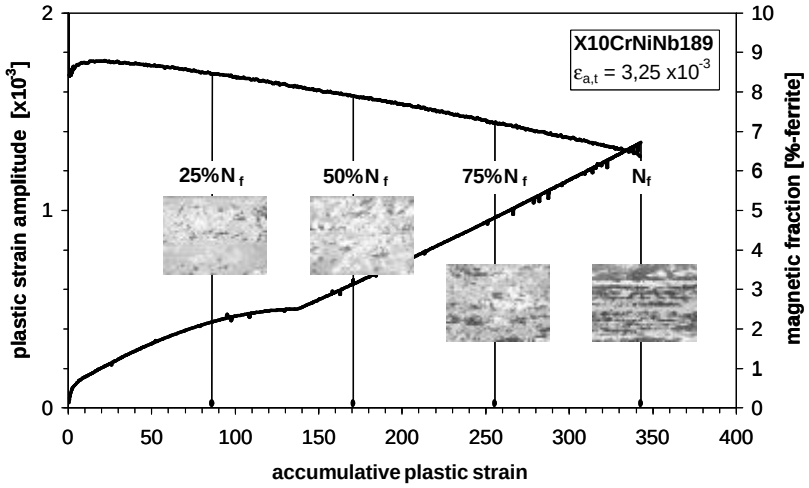

Figure 23. Microstructure of X10CrNiNb189 at $3{\cdot}25 \times 10^{-3}$.

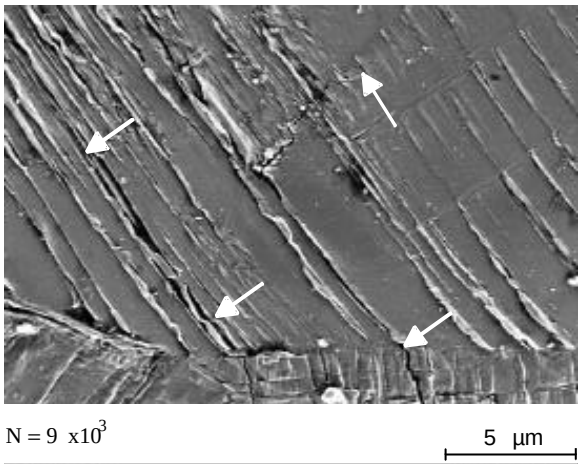

Figure 24. Micro-cracks in the austenite of X6CrNiTi1810 at ambinent temperature ($\sigma_a = 380$ MPa).

values rise from 7 to 9, 15 and 47 area-%. This different in the formation of martensite formation could be attributed to the smaller austenite-destabilizing effect of the alloying element titanium and to the reduced carbon and Ni-content of the steel X10CrNiNb189.

The influence of the test temperature on the development of characteristic surface features is explained below in the steel X6CrNiTi1810 (virgin state). The surfaces of flat specimens cycled at 380 MPa (ambient temperature) or 280 MPa (300°C) were examined continuously after defined numbers of cycles in a scanning electron microscope. At ambient temperature the stress amplitude 380 MPa introduces plastic deformation after a few cycles and first slip lines are observed in the austenitic phase. The first martensite structures are determined after 10^3 cycles at the beginning of the cyclic softening followed by micro-cracks in the austenite and martensite (see figure 24).

Combined with the cyclic hardening a pronounced increase of the martensite phase transformation is observed. Extrusions and intrusions occur and the macro-crack propagation starts after $1{\cdot}2 \times 10^4$ cycles (see figure 25).

An increase of the test temperature causes a distinct modification of the cyclic deformation behaviour (compare Sandhya *et al* 2001 and Srinivasan *et al* 1999). Apart from decreasing numbers of cycles to failure the cyclic deformation curves in comparison to ambient temperature do not indicate pronounced cyclic hardening at the same load levels. At 300°C and about 10^3 cycles slip lines are observed in the austenitic phase. After $1{\cdot}2 \times 10^4$ cycles slip bands and martensite structures have been detected (see figure 26).

During the softening of the steel after 4×10^4 cycles extrusions and first micro-cracks occur in the slip bands (see figure 27).

Since the martensite contents at $T = 300$°C are very small compared with ambient temperature, fewer cracks occur but they can propagate in an easier way.

5. Conclusions

Steels 1·4541 (X6CrNiTi1810), 1·4546 (X10CrNiNb189) and 1·4301 (X5CrNi1810) were investigated to characterise the cyclic deformation behaviour and the plasticity-induced martensite formation at ambient and elevated temperatures.

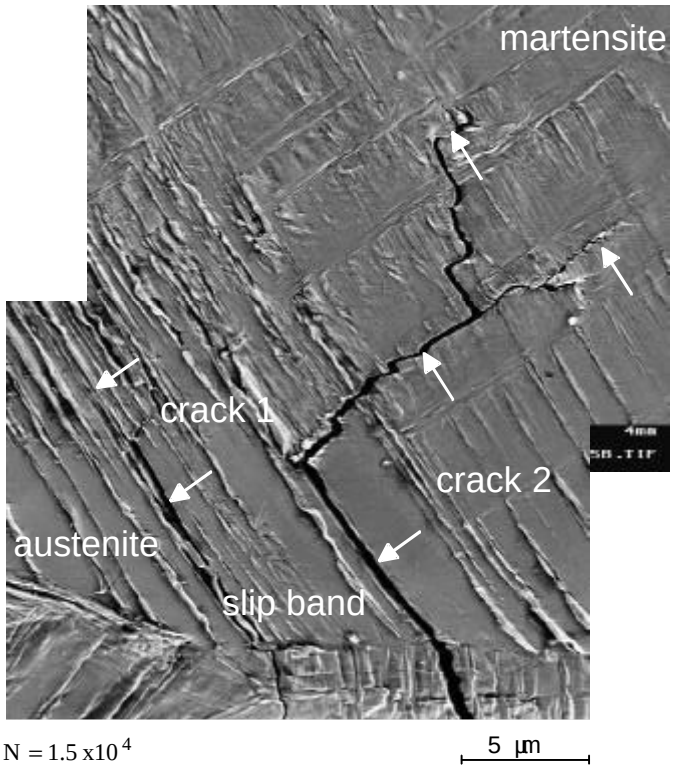

Figure 25. Micro-crack propagation in the martensite of X6CrNiTi1810 at ambinent temperature ($\sigma_a = 380$ MPa).

- Fatigue behaviour is characterised by cyclic hardening and softening effects which are strongly influenced by the specific loading conditions. Martensite formation varies with the composition, loading conditions, temperature and number of cycles.

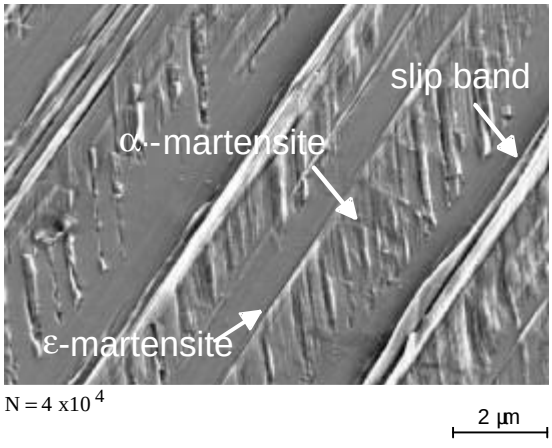

Figure 26. Martensite structures on the surface of X6CrNiTi1810 at $T = 300°$C ($\sigma_a = 280$ MPa).

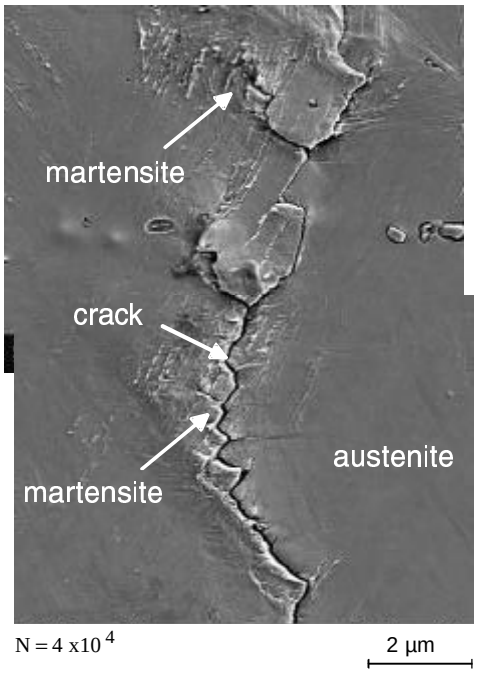

Figure 27. Divided cracks on the surface of X6CrNiTi1810 at $T = 300^{\circ}$C ($\sigma_a = 280$ MPa).

- Under total-strain control all three solution annealed steels show almost comparable cyclic deformation behaviour. Under stress control the endurance limit of 1·4546 is somewhat higher than the one of 1·4541 followed by 1·4301.
- Positive mean stresses lead to higher plastic-strain amplitudes and decreasing number of cycles to failure, negative mean stresses lead to lower plastic-strain amplitudes and consequently increasing numbers of cycles to failure. The development of the martensite fraction ratio shows the same dependencies and is comparable to tests without mean stresses.
- Under total-strain control a significant influence of positive or negative mean strains on the martensite formation could not be determined, due to the fast and nearly complete relaxation of the mean stresses.
- In case of total-strain control it is necessary to replace the stress in the CSS-Curves with the actual controlled variable to get C_{yclic} T_{otal} S_{train} S_{tress}-Curves with as expected higher plastic-strain amplitudes with increasing total-strain amplitudes.
- The C_{yclic} S_{tress} $T_{emperature}$-Curves and C_{yclic} T_{otal} S_{train} $T_{emperature}$-Curves underline the applicability of the temperature measurement for the quantitative description of the cyclic deformation behaviour.
- SQUID-measurements supply a unique dependency of the magnetic field values on the number of cycles. The measured values are clearly higher for samples, which were loaded at ambient temperature. This reflects the different martensite contents at different test temperatures.
- Measurements of the GMR-impedance show a clear correlation between the plastic-strain amplitude and the martensite formation.

References

Bassler H-J, Dobmann G, Lang M, Eifler D 1997 Characterization of the fatigue behaviour of austenitic steel using HTSL-Squid. *23th Annual Review of Progress in Quantitative Nondestructive Evaluation*, San Diego, USA, pp 1597–1604

Bayerlein M, Christ H-J, Mughrabi H 1989 Plasticity induced martensitic transformation during cyclic deformation of AISI 304L stainless steel, *Mater. Sci. Eng.* A114: L11–L16

Dobmann G, Lang M, Eifler D, Bassler H-J 2001 On-line Fatigue Monitoring of Austenitic Stainless Steel Using a GMR-Sensor. *6th Int. Workshop on Electromagnetic Nondestructive Evaluation* (Budapest: IOS Press) pp 259–266

Eckstein H-J 1990 Korrosionsbeständige Stähle. *Deutscher Verlag für Grundstoffindustrie* (Leipzig) pp 90–98

Eifler D 1997 Fatigue behaviour of steel at ambient and elevated temperatures. In *Risk based assessment of industrial components and plants - vol. II. QUNEST and Q NET* (Madras: Indian Institute of Technology) pp 1–17

Eifler D 2000 Fatigue behaviour of ferritic and austenitic steels at elevated temperatures. *Materials ageing and life management* (ed.) Sunil Sachdev (Kalpakkam: Allied Publishers) vol. 1 pp 17–26

Harig H, Dengel D 1980 Estimation of the fatigue limit by progressively-increasing load tests, *Fatig. Eng. Mater. Struct.* 3: pp 113–128

Lang M, Johnson J, Schreiber J, Dobmann G, Bassler H J, Eifler D, Ehrlich R, Gampe U 2000 Cyclic deformation behaviour of AISI 321 austenitic steel and its characterization by means of HTC-SQUID. *Nucl. Eng. Design* 198: pp 185–191

Nebel T, Martin U, Eifler D 2001 Wechselverformungsverhalten metastabiler austenitischer Stähle. *HTM Härterei-Technische Mitteilungen, Zeitschrift für Wärmebehandlung und Werkstofftechnik* (München: Carl Hanser Verlag) HTM 56, pp 314–320

Olsen G B, Cohen M 1975 Kinetics of strain induced martensite nucleation. *Metall. Trans.* A6: 791–795

Sandhya R, Bhanu Sankara Rao K, Mannan S L, Devanathan R 2001 Substructural recovery in a cold worked Ti-modified austenitic stainless steel during high temperature low cycle fatigue. *Int. J. Fatig.* 23: 789–797

Srinivasan V S, Valsan M, Sandhya R, Bhanu Sankara Rao K, Mannan S L, Sastry D H 1999 High temperature time-dependent low cycle fatigue behaviour of a 316L(N) stainless steel. *Int. J. Fatig.* 21: 11–21